Influence of adhesion between the main cement phases on the mechanical behavior of hydrated cement paste

Sela HOEUN

Nantes Université, École Centrale Nantes, CNRS, GeM, UMR 6183, F_44000 Nantes, France

Université de Rennes, INSA Rennes, LGCGM, 20 avenue des Buttes de Coësmes 35700 Rennes, France

RESUME Cette étude porte sur la modélisation multi-échelle des propriétés mécaniques des matériaux cimentaires. L'objectif est d'acquérir les propriétés mécaniques des phases de la pâte de ciment hydratée à l'échelle nanométrique, en utilisant des simulations de Dynamique Moléculaire. En effet, les données obtenues à l'échelle inférieure (échelle nanométrique) sont considérées comme les paramètres d'entrée à l'échelle supérieure (échelle microscopique). À l'échelle nanométrique, des essais de traction ont été menés sur les principales phases de la pâte de ciment hydratée, notamment les hydrates de silicate de calcium et la portlandite. La combinaison de ces deux phases a été désignée comme "composite de pâte de ciment" dans cette étude. Les configurations d'espacement et les orientations des composites de pâte de ciment ont été examinées pour différents scénarios. Ainsi, les propriétés mécaniques à l'échelle nanométrique ont été déterminées. Les résultats indiquent que les courbes contrainte-déformation étaient affectées à la fois par les orientations et les configurations d'espacement. Un comportement fragile ou ductile, plus ou moins d'oscillations et des contraintes maximales plus ou moins importantes peuvent être observées dans différents cas.

Mots-clefs Modélisation multi-échelle, Pâte de ciment hydratée, Dynamique Moléculaire

I. INTRODUCTION

Cementitious materials are the most used materials that are characterized by a heterogeneous composition on multiple scales. Behavior of concrete and especially its cracking remain relatively poorly controlled due to this complex structure. Concrete is a complex composite consisting of aggregates (particulate phase) and cement matrix (binding phase). Therefore, the mechanical properties of concrete are significantly influenced by the cement matrix (Keinde et al., 2014; Lau et al., 2018). Moreover, cement paste is a porous multiscale substance with varying physical properties across different length scales (Ioannidou, 2020). Calcium-silicate-hydrates (C-S-H) comprising up to 50% of the volume is the major component of hardened hydrated cement paste (Lau et al., 2018). Another substantial phase in hydrated Portland cement paste is portlandite (CH), typically constituting 15-25% of the ignited mass in pastes of typical Portland cements cured for 3-12 months (Taylor, 1997).

For multi-scale modelling, obtaining the mechanical properties of various phases of hydrated cement paste is essential. Nano-indentation experiments (Fu, Kamali-Bernard, et al., 2018) is one of

a method to acquire these properties. Nonetheless, values obtained by nano-indentation tests could be untrustworthy. Hence, it leads to obtain these properties by other method, for instance, numerical simulation (i.e., Molecular Dynamics (MD) simulation at the nano-scale). Indeed, it is now necessary to grasp the adhesion properties between different hydrated cement paste phases and to consider them at the microstructure scale of the cement paste. The rupture of adhesion between these phases is the primary cause of material damage and micro-cracking, often more significant than the rupture of the phases themselves (inter-phase rather than intra-phase ruptures) (Del Gado et al., 2014; Manzano et al., 2009, 2013; Zhou et al., 2017).

The two main objectives of this study are as follows: (1) obtain the mechanical properties of interphases of the main cement paste phases, for example by mean of modelling via MD simulations and (2) use results obtained from MD simulations as the inputs in the scale of hardened cement paste (i.e., micro-scale) by mean of Discrete Element Method. This study may make it possible to create the bridge of achieving the transition from molecular scale to microscopic scale.

This article focuses primarily on the mechanical properties calculation of hydrated cement phase composites using MD simulations at the nano-scale. In fact, mechanical properties of different phase composites are required for the multi-scale modelling. The results obtained in this article could be served as the inputs in the upper-scale, i.e., microscale of cement-based materials. We used MD simulations with ReaxFF force field to investigate the mechanical properties of these composites. Two main hydrated cement paste phases have been chosen to study. Those phases are C-S-H (I) and CH. In this study, different phases put together are called “composite” (i.e., C-S-H (I)/CH composite). Three different orientations and spacing configurations were imposed on these composites. Tensile tests were performed on these composites with strain rate of 10^{-6} fs^{-1}. Stress-strain curves were then obtained. As a result, Young’s modulus, peak stress and peak strain could be deduced from these stress-strain curves. The contents of this article were placed in the following order: (a) Materials, (b) Method, (c) Results and Discussion, and (d) Conclusion.

II. MATERIALS

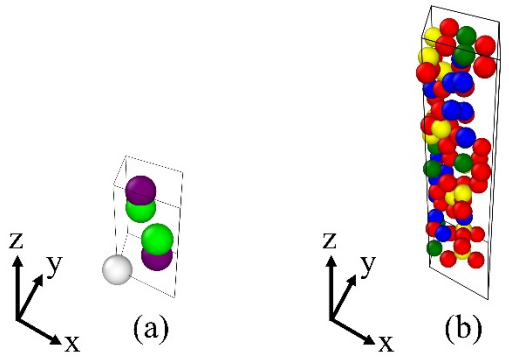

FIGURE 1. Perspective view of (a) portlandite (CH) and (b) 11 Å tobermorite unit cells.

The formation of calcium hydroxide (CH) generally occurs in conjunction with the hydration of C_3S or C_2S phases (Hewlett, 1998). In this article, unit cell of portlandite (CH) was modelled following

(Desgranges et al., 1993) as shown in **Figure 1a** with the chemical formula $Ca(OH)_2$ and cell angles (α, β, γ) = (90°, 90°, 120°). Cell lengths are (a, b, c) = (3.589 Å, 3.589 Å, 4.911 Å). White balls are Ca atoms, lime balls are H atoms, and purple balls are O atoms. Crystal structure is trigonal in the $P\bar{3}m1$ space group. OVITO (Open Visualization Tool) (Stukowski, 2009) was used for the visualization of all simulations.

Amorphous or nearly amorphous C-S-H products are referred to as the 'C-S-H phase.' When C_3S hydrates at room temperature, it produces the C-S-H phase, structurally related to crystalline phases like 1.1 nm tobermorite and jennite, as well as weakly crystalline substances C-S-H (I) and C-S-H (II) (Hewlett, 1998). C-S-H phase is generally amorphous with no long-range order. Based on the ratio of Ca/Si, C-S-H phase can be grouped into calcium-rich and into silicon-rich forms and can also be grouped into C-S-H (I) with Ca/Si ratio of 0.6-1.5 and C-S-H (II) with Ca/Si ratio of 1.5-2.0. Both C-S-H (I) and C-S-H (II) structures resemble tobermorite with the exception of which some silicon oxygen tetrahedrons in their silicon chain are partially lost or deformed and hence form some plurality of dimmers (Fu, Bernard, et al., 2018). In the study of (Fu, Bernard, et al., 2018), they developed C-S-H cell starting from tobermorite 11 Å and obtained first amorphous tobermorite whose long range is distorted. Unit cell of 11 Å tobermorite was obtained from work of (Fu, Bernard, et al., 2018). It has chemical formula $Ca_4Si_6O_{14}(OH)_4{\cdot}2H_2O$, cell angles ($\alpha$, β, γ) = (90°, 90°, 123.49°) and cell lengths (a, b, c) = (6.69 Å, 7.39 Å, 22.779 Å). Crystal structure is monoclinic in the $P2_1$ space group. C-S-H was modelled based on (Hamid, 1981) as can be seen in **Figure 1b**. Green balls are Ca atoms, yellow balls are Si atoms, red balls are O atoms, and blue balls are H atoms. (Fu, Bernard, et al., 2018) developed C-S-H (I) initially from 11 Å tobermorite with annealing process. Following the same procedure, we obtained C-S-H (I) with Ca/Si ratio of 0.67.

Molecular Dynamics using in this study is a computer simulation technique for analyzing physical movement of atoms and molecules. Atoms and molecules can interact for a time period, giving insight into dynamic evolution of the system. In the most common version, atoms and molecules trajectories are determined by numerically solving Newton's equation of motion in a system of interacting particles. The interatomic force and its potential energy are often calculated using the interatomic potential or the mechanical force field of the molecules (Plimpton, 1995).

Large-scale Atomic/Molecular Massively Parallel Simulator (LAMMPS) was utilized to perform the simulations. LAMMPS focuses on material modelling using a classical molecular dynamics code. It can be used for soft matters, solid-state materials, and coarse-grained or mesoscopic systems to model atoms as a parallel particle simulator at continuum, meso or atomic scale. It is an opened source code which distributed by Sandia National Laboratories, a US department of energy laboratory under the terms of GPL. In order to compute their motion, Newton's equations are integrated while each of N atoms or molecules in the simulation is considered as a point mass (Plimpton, 1995).

ReaxFF force field is the force field using in this study because ReaxFF force field could be used with all the phases of hydrated cement paste that we intended to study (i.e., not only calcium-silicate-hydrates and portlandite but also ettringite (Hoeun, 2023)). (van Duin et al., 2001) developed ReaxFF force field for hydrocarbons, which is a force field for reactive systems in order to make practical molecular dynamics simulations of large scale reactive chemical systems. On the one hand, ReaxFF force field uses a general relationship between bond order and bond distance.

On the other hand, ReaxFF force field uses a general relationship between bond order and bond energy, which leads to proper dissociation of bonds to separate atoms. From reactions of small molecules plus geometry data and heat of formation for a number of stable hydrocarbon compounds and quantum chemical calculations on bond dissociation, the parameters were derived. ReaxFF parameters using in this study could be found in (Liu et al., 2012).

System energy of ReaxFF force field could be written as follows (van Duin et al., 2001):

$$E_{system} = E_{bond} + E_{over} + E_{under} + E_{val} + E_{pen} + E_{tors} + E_{conj} + E_{vdWaals} + E_{Coulomb} \quad (1)$$

where E_{bond} represents the bond energy, E_{over} and E_{under} the energy penalty for over- and under-coordination of atoms, E_{val}, E_{pen}, E_{tors}, E_{conj}, $E_{vdWaals}$ and $E_{Coulomb}$ the valence angle, penalty, torsion, conjugation, van der Waals and Coulomb energy, respectively.

III. METHOD

In the work of (Liang, 2020), mechanical and fracture properties of C-S-H/CH composites were investigated. In order to get representative results, C-S-H and CH unit cells were extended along x-, y-, and z-directions. Supercells were then relaxed with NPT ensemble at temperature of 300 K and pressure of 0 Pa at x-, y- and z-directions. Relaxed supercells were put together with about 3 Å gap. C-S-H/CH composites was relaxed once again with NPT ensemble.

Similar to the methodology proposed by (Liang, 2020), unit cells of C-S-H (I) and CH were replicated in x-, y-, and z-directions. Size of supercells was chosen to ensure that all chosen phases (i.e., C-S-H (I) and CH) have a similar size in all three dimensions. C-S-H (I) unit cell was replicated by 7 × 8 × 2 in x-, y- and z-directions, respectively. CH unit cell was replicated by 13 × 16 × 9 in x-, y- and z-directions, respectively. C-S-H (I) and CH supercells were changed from monoclinic and trigonal supercells to orthogonal supercell in order to acquire the independent results to each direction. All MD simulations were done with ReaxFF force field in real units and three dimensions (3D). To eliminate boundary effect during simulation, periodic boundary condition (PPP) was utilized. These supercells were relaxed in NPT ensemble with temperature of 300 K and pressure of 0 atm in all three directions for a period of 50 ps. Tensile tests were performed on these composites with strain rate of 10^{-6} fs^{-1}.

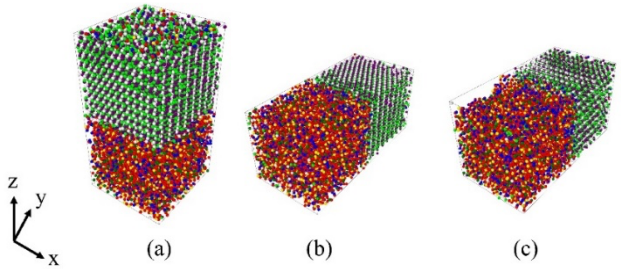

FIGURE 2. Orientations of C-S-H (I)/CH composites: (a) in z-direction, (b) in y-direction, and (c) counterclockwise rotated in y-direction.

(Bonnaud et al., 2016) investigated three different orientations of C-S-H particle pairs in order to study the interaction grand potential at the molecular level. Different orientations was chosen because these orientations could take into account the effect of anisotropy in crystallography and geometry of C-S-H particles. Morever, different interaction forces among particles was related to orientation. Similarly, three different orientations were chosen in this study as follows: (a) CH supercell on top of C-S-H (I) supercell in z-direction, (b) CH supercell at the side of C-S-H (I) supercell in y-direction, and (c) counterclockwise rotated CH supercell around x-axis at the side of C-S-H (I) supercell in y-direction. In the latter case, bottom of CH supercell was placed at the side of C-S-H (I) supercell. **Figure 2** shows the different orientations. Additionally, 1 Å vacuum, 3.1 Å water and 6.2 Å water spacing were placed between relaxed C-S-H (I) and CH supercells. On the one hand, 1 Å vacuum spacing referred to an interface without porosity in between two phases. On the other hand, 3.1 and 6.2 Å water spacing referred to the interface with porosity filled with water in between two phases. C-S-H (I)/CH composites were relaxed once again with NPT ensemble for another 50 ps. Timestep of these simulations was 0.25 fs. Deformations were applied along y- or z-directions coupled with relaxation in lateral directions.

To conduct simulations on C-S-H (I)/CH composites, 24 visualization cores were employed. The computational setup included the use of a supercomputer named "Liger," equipped with 12-core Intel Xeon (Haswell) E5-2680v3 processors. The supercomputer comprised 252 compute nodes, each with 24 cores, along with 14 visualization nodes featuring 28 GPUs and 24 cores per node. The memory capacity was 36,608 GB.

IV. RESULTS AND DISCUSSION

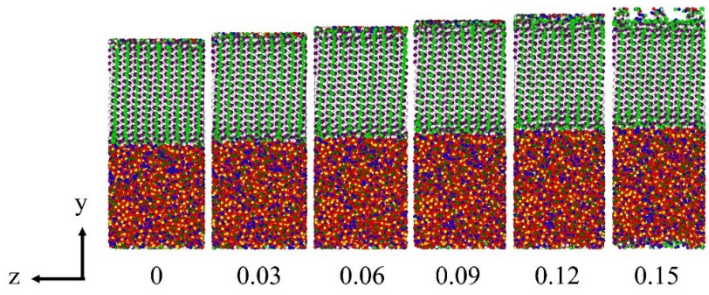

FIGURE 3. **Direct tension of C-S-H (I)/vacuum (1 Å)/CH composites in y-direction.**

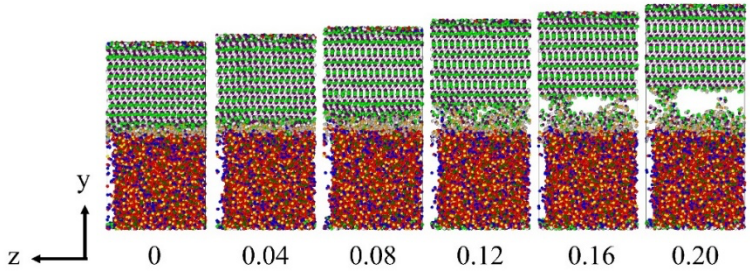

FIGURE 4. **Direct tension of C-S-H (I)/H_2O (3.1 Å)/CH composites counterclockwise rotated in y-direction.**

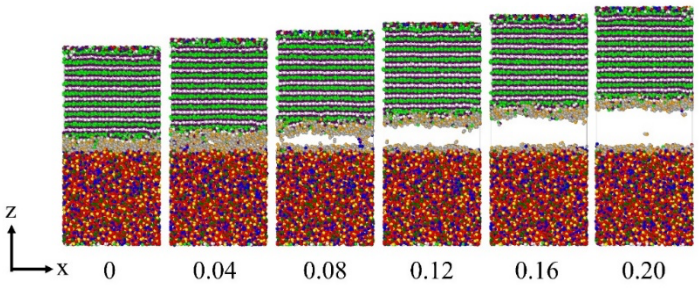

FIGURE 5. **Direct tension of C-S-H (I)/H_2O (6.2 Å)/CH composites in z-direction.**

In the case of C-S-H (I)/CH composites with ReaxFF force field, **Figure 3** - **Figure 5** illustrate the direct tensile evolution of C-S-H (I)/CH composites after relaxation to 15% and 20% strain with different orientations and spacing configurations. All simulations were run with the strain rate of 10^{-6} fs^{-1}. All rupture appeared at the interface of composites indicating that vacuum and water spacing made interaction between main hydrated cement phases weaker and initiated the rupture.

Stress-strain curves of C-S-H (I)/CH composites with different orientations and spacing configurations can be observed in **Figure 6** - **Figure 8**. In the case of 1 Å vacuum spacing, the behavior seems to be ductile. For orientation in y-direction, it gave a bigger peak stress and peak strain compared to the other orientations. It indicates that this orientation provided a better interaction at the interface between C-S-H (I) and CH supercells. In the case of 3.1 Å water spacing, the behavior seems to be ductile too. In the case of 6.2 Å water spacing, the behavior seems to be more brittle compared to the smaller spacing. It appears that the bigger the spacing, the bigger the oscillation can be observed. Results indicate that orientations of two supercells and spacing configurations affected the stress-strain curves of C-S-H (I)/CH composites. As can be seen, 1 Å vacuum spacing gave the highest peak stress and peak strain. In contrast, 6.2 Å water spacing gave the lowest peak stress and peak strain. Results of peak strain, peak stress, Young's modulus and running time are summarized in **Table 1**.

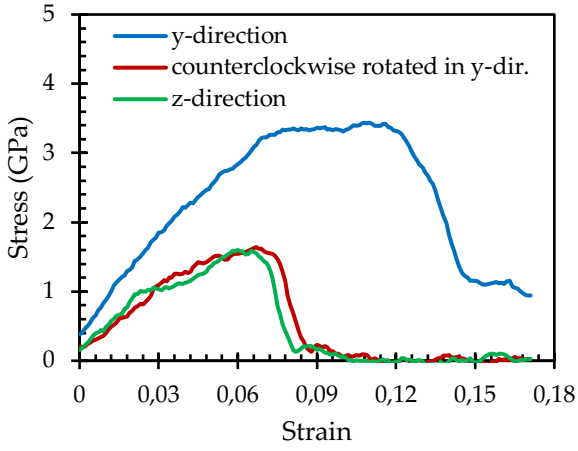

FIGURE 6. **Stress-strain curves of C-S-H (I)/CH composites with 1 Å vacuum spacing.**

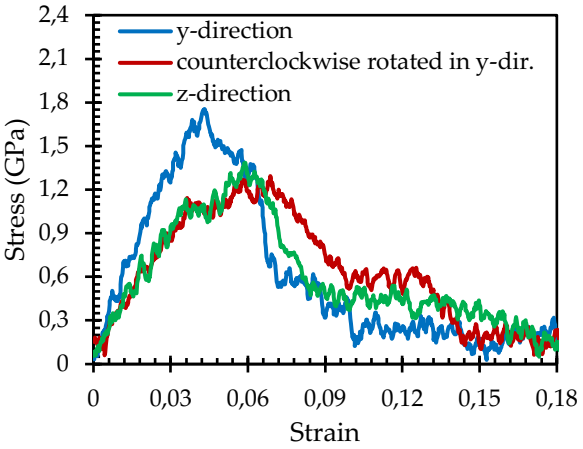

FIGURE 7. **Stress-strain curves of C-S-H (I)/CH composites with 3.1 Å water spacing.**

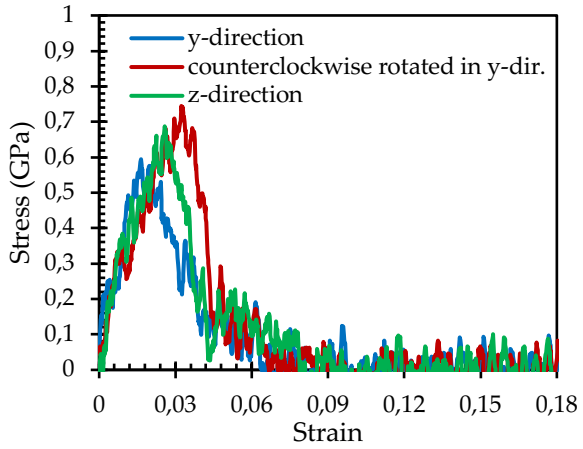

FIGURE 8. **Stress-strain curves of C-S-H (I)/CH composites with 6.2 Å water spacing.**

TABLE 1. **Peak strain, peak stress, Young's modulus and running time of C-S-H (I)/CH composites.**

Orientation	Spacing	Peak strain	Peak stress (GPa)	Young's modulus (GPa)	Running time (hr:min)
y-direction	1 Å vacuum	0.11	3.44	48.6	72:00
	3.1 Å water	0.04	1.75	44.9	47:54
	6.2 Å water	0.02	0.59	39.1	49:46
Counterclockwise rotated in y-direction	1 Å vacuum	0.07	1.64	29.7	72:00
	3.1 Å water	0.07	1.29	29.7	45:36
	6.2 Å water	0.03	0.74	39.3	48:12
z-direction	1 Å vacuum	0.06	1.60	33.5	72:00
	3.1 Å water	0.06	1.39	31.1	44:39
	6.2 Å water	0.03	0.69	39.1	48:13

Average Young's moduli of three different orientations are summarized in **Table 2**. In the case of 1 Å vacuum spacing, Young's modulus was found to be 37.3 GPa for C-S-H (I)/CH composite. When 3.1 Å water spacing was placed in between the supercells, Young's modulus decreased to 35.2 GPa. Finally, Young's modulus were found to be 39.1 GPa for 6.2 Å water spacing. To the author's knowledge, C-S-H (I)/CH composites modelled with MD simulation was only done by (Liang, 2020). The values of Young's modulus might be compared to the result obtained by Liang, 2020) with value of 40 GPa. The procedure is quite similar to this study. Liang placed CH phase about 3 Å on top of C-S-H phase and derived the Young's modulus from the stress-strain curve of uniaxial tensile test.

TABLE 2. Mean Young's modulus of three different orientations of C-S-H (I)/CH composites.

Composite	Spacing	Young's modulus (GPa)
C-S-H (I)/CH	1 Å vacuum	37.3
	3.1 Å water	35.2
	6.2 Å water	39.1

In summary, tensile tests were applied on the main cement phase composites. These simulations provided the stress-strain curves of composites. As a result, peak strain, peak stress, and Young's modulus could be calculated from the stress-strain curves. For spacing configurations, 1 Å vacuum spacing has the highest peak stress, followed by 3.1 Å and 6.2 Å water spacing. All ruptures appeared at the interface of composites indicating that vacuum and water spacing made the interaction between main hydrated cement phases weaker and initiated the rupture. These results can be served in the upper-scale simulation as the inputs, for instance, in the scale of hardened cement paste (i.e., micro-scale) by mean of Discrete Element Method.

V. CONCLUSION

The aim of this study was to investigate the mechanical properties of different phases of hydrated cement paste required for multi-scale modelling. Numerical simulations, i.e., via Molecular Dynamics simulations at the nano-scale, could be used to obtain these properties. The grasp of adhesion properties between different hydrated cement paste phases is important because the rupture of adhesion between these phases is responsible for the damage of material and micro-cracking even more than the rupture of the phases themselves (inter-phase and not intra-phase ruptures). Adhesion between main hydrated cement paste phases of C-S-H (I) and CH was taken into account by means of Reactive MD simulations with ReaxFF force field. Combination of two different main phases of hydrated cement paste was called "cement paste composite" in this study. Three different orientations and spacing configurations were imposed. Those orientations are as follows: (a) CH phase on the top of C-S-H (I) phase in z-direction, (b) CH phase at the side of the C-S-H (I) phase in y-direction, and (c) counterclockwise rotated CH phase around x-axis at the side of C-S-H (I) phase in y-direction. For spacing configurations, they are as follows: (a) 1 Å vacuum spacing, (b) 3.1 Å water spacing and (c) 6.2 Å water spacing. Spacing was placed in-between the relaxed C-S-H (I) and CH phases. Results indicate that stress-strain curves were affected by both

orientations and spacing configurations. Brittle or ductile behavior, more or less oscillation, and bigger or smaller peak stress can be observed for different cases.

In conclusion, this work demonstrates the feasibility of using Molecular Dynamics simulations in order to obtain mechanical interphase properties of main hydrated cement paste phases. Moreover, our results could be served as the inputs to access the mechanical properties of hardened cement paste by means of Discrete Elements Method, for example. Therefore, this work makes it possible to create the bridge of achieving the transition from molecular scale to microscopic scale. Future work should include the development of ReaxFF force field that will be optimized for all the hydrated cement paste phases because ReaxFF force field developed for ettringite was used in this study. It is possible to use this method to obtain the mechanical properties of different composites between other hydrated and unhydrated phases.

REFERENCES

Bonnaud, P. A., Labbez, C., Miura, R., Suzuki, A., Miyamoto, N., Hatakeyama, N., Miyamoto, A., & Vliet, K. J. V. (2016). Interaction grand potential between calcium–silicate–hydrate nanoparticles at the molecular level. *Nanoscale*, *8*(7), 4160–4172. https://doi.org/10.1039/C5NR08142D

Del Gado, E., Ioannidou, K., Masoero, E., Baronnet, A., Pellenq, R. J.-M., Ulm, F.-J., & Yip, S. (2014). A soft matter in construction – Statistical physics approach to formation and mechanics of C–S–H gels in cement. *The European Physical Journal Special Topics*, *223*(11), 2285–2295. https://doi.org/10.1140/epjst/e2014-02264-1

Desgranges, L., Grebille, D., Calvarin, G., Chevrier, G., Floquet, N., & Niepce, J.-C. (1993). Hydrogen thermal motion in calcium hydroxide: Ca(OH)2. *Acta Crystallographica Section B: Structural Science*, *49*(5), Article 5. https://doi.org/10.1107/S0108768193003556

Fu, J., Bernard, F., & Kamali-Bernard, S. (2018). Assessment of the elastic properties of amorphous calcium silicates hydrates (I) and (II) structures by molecular dynamics simulation. *Molecular Simulation*, *44*(4), 285–299. https://doi.org/10.1080/08927022.2017.1373191

Fu, J., Kamali-Bernard, S., Bernard, F., & Cornen, M. (2018). Comparison of mechanical properties of C-S-H and portlandite between nano-indentation experiments and a modeling approach using various simulation techniques. *Composites Part B: Engineering*, *151*, 127–138. https://doi.org/10.1016/j.compositesb.2018.05.043

Hamid, S. A. (1981). The crystal structure of the 11Å natural tobermorite Ca2.25[Si3O7.5(OH)1.5] · 1H2O. *Zeitschrift Für Kristallographie - Crystalline Materials*, *154*(3–4), 189–198. https://doi.org/10.1524/zkri.1981.154.3-4.189

Hewlett, P. C. (1998). *Lea's Chemistry of Concrete and Cement*. Elsevier, Oxford.

Hoeun, S. (2023). *Influence de l'adhésion entre les principales phases cimentaires sur le comportement mécanique de la pâte de ciment hydratée* [PhD Thesis]. Nantes, Ecole Centrale de Nantes.

Ioannidou, K. (2020). Mesoscale Structure and Mechanics of C-S-H. In W. Andreoni & S. Yip (Eds.), *Handbook of Materials Modeling: Applications: Current and Emerging Materials* (pp. 1–15). Springer International Publishing. https://doi.org/10.1007/978-3-319-50257-1_127-1

Keinde, D., Kamali-Bernard, S., Bernard, F., & Cisse, I. (2014). Effect of the interfacial transition zone and the nature of the matrix-aggregate interface on the overall elastic and inelastic behaviour of concrete under compression: A 3D numerical study. *European Journal of Environmental and Civil Engineering*, *18*(10), 1167–1176. https://doi.org/10.1080/19648189.2014.896757

Lau, D., Jian, W., Yu, Z., & Hui, D. (2018). Nano-engineering of construction materials using molecular dynamics simulations: Prospects and challenges. *Composites Part B: Engineering*, *143*, 282–291. https://doi.org/10.1016/j.compositesb.2018.01.014

Liang, Y. (2020). Mechanical and fracture properties of calcium silicate hydrate and calcium hydroxide composite from reactive molecular dynamics simulations. *Chemical Physics Letters*, *761*, 138117. https://doi.org/10.1016/j.cplett.2020.138117

Liu, L., Jaramillo-Botero, A., Goddard, W. A., & Sun, H. (2012). Development of a ReaxFF Reactive Force Field for Ettringite and Study of its Mechanical Failure Modes from Reactive Dynamics Simulations. *The Journal of Physical Chemistry A*, *116*(15), 3918–3925. https://doi.org/10.1021/jp210135j

Manzano, H., Dolado, J. S., & Ayuela, A. (2009). Elastic properties of the main species present in Portland cement pastes. *Acta Materialia*, *57*(5), 1666–1674. https://doi.org/10.1016/j.actamat.2008.12.007

Manzano, H., Masoero, E., Lopez-Arbeloa, I., & Jennings, H. M. (2013). Shear deformations in calcium silicate hydrates. *Soft Matter*, *9*(30), 7333–7341. https://doi.org/10.1039/C3SM50442E

Plimpton, S. (1995). Fast Parallel Algorithms for Short-Range Molecular Dynamics. *Journal of Computational Physics*, *117*(1), 1–19. https://doi.org/10.1006/jcph.1995.1039

Stukowski, A. (2009). Visualization and analysis of atomistic simulation data with OVITO–the Open Visualization Tool. *Modelling and Simulation in Materials Science and Engineering*, *18*(1), 015012. https://doi.org/10.1088/0965-0393/18/1/015012

Taylor, H. F. W. (1997). *Cement chemistry* (2. ed., Repr). Telford.

van Duin, A. C. T., Dasgupta, S., Lorant, F., & Goddard, W. A. (2001). ReaxFF: A Reactive Force Field for Hydrocarbons. *The Journal of Physical Chemistry A*, *105*(41), 9396–9409. https://doi.org/10.1021/jp004368u

Zhou, Y., Hou, D., Manzano, H., Orozco, C. A., Geng, G., Monteiro, P. J. M., & Liu, J. (2017). Interfacial Connection Mechanisms in Calcium–Silicate–Hydrates/Polymer Nanocomposites: A Molecular Dynamics Study. *ACS Applied Materials & Interfaces*, *9*(46), 41014–41025. https://doi.org/10.1021/acsami.7b12795